An empirical investigation of source term balance of small scale surface waves

Paul A. Hwang and David W. Wang

Oceanography Division, Naval Research Laboratory, Stennis Space Center, Mississippi, USA

Received 25 March 2004; accepted 9 July 2004; published 3 August 2004.

[1] *Phillips* [1984] presents a method to derive the dissipation function (D) of the wave action density conservation equation from the functional dependence of the wave saturation spectrum (B) on wind friction velocity. The method is applied to field spectra of small scale waves (wavelengths between 0.02 and 6 m). The results indicate that D approaches asymptotically to B^3 toward long gravity waves and to $B^{2.3}$ for short gravity waves. In the middle wavelength range (0.16 to 2.1 m), the dependence is as strong as B^{10}. This may suggest that the spectral property of wave breaking is localized in the wavenumber space, with strong signature in the 0.16 to 2.1 m wavelength scale. *INDEX TERMS:* 4560 Oceanography: Physical: Surface waves and tides (1255); 4504 Oceanography: Physical: Air/sea interactions (0312); 4572 Oceanography: Physical: Upper ocean processes; 4594 Oceanography: Physical: Instruments and techniques. **Citation:** Hwang, P. A., and D. W. Wang (2004), An empirical investigation of source term balance of small scale surface waves, *Geophys. Res. Lett.*, *31*, L15301, doi:10.1029/2004GL020080.

1. Introduction

[2] For wind generated waves, the dissipation source term remains the most difficult to be formulated. The problem is further exacerbated by the fact that measurement and quantification of wave breaking is a very difficult task. *Phillips* [1984] describes an approach to establish the dissipation function, D, in the equilibrium region of gravity waves from the functional dependence of the saturation spectrum, B, on u_*/c, the ratio of wind friction velocity and wave phase speed, assuming local balance between the wind input and wave dissipation in the equilibrium region, and employing an empirically established wind input function.

[3] The method is applied to several field datasets of small scale surface wave measurements obtained by an array of fast response wave gauges. It is found that B can be expressed as a power-law function of u_*/c. The exponent is close to one for gravity waves with wavelength longer than about three meters, it drops to about 0.25 in the meter-wavelength range, and gradually increases to about 1.5 at the shorter end of the gravity wave spectrum. Assuming that D can be expressed as a power-law function of B [*Phillips*, 1984], the coefficient and exponent of $D(B)$ can be obtained from the coefficient and exponent of $B(u_*/c)$. The calculated exponent of $D(B)$ is about three for long gravity waves and two for short gravity waves. In the middle wavelength range (wavelength, λ, between about 0.16 and 2.1 m), the exponent is considerably larger and reaches above 10 in the neighborhood of 1-m long wavelength components.

[4] In the following, Section 2 summarizes Phillips' approach to quantify the dissipation function from the knowledge of $B(u_*/c)$. Section 3 describes the field experiment and data processing. Section 4 presents the analysis results, with discussions given in Section 5. Section 6 is summary and conclusions.

2. Balance of Source Functions

[5] The balance of wave action spectral density of surface waves, $N(\boldsymbol{k})$, can be expressed as

$$\frac{dN}{dt} = -\frac{\partial T_i}{\partial k_i} + S_w - D, \tag{1}$$

where $\boldsymbol{k}$ is wavenumber. The three terms on the right hand side of equation (1) represent the source functions due to wave-wave interaction, wind input and dissipation. N is related to the wave displacement spectral density, Ψ, by $N = g\Psi/\sigma$, g is gravitational acceleration, and σ is the intrinsic frequency of the wave field.

[6] As summarized by *Phillips* [1984], theoretical and experimental studies of the energy transfer from wind to waves have led to the following parameterization function for the wind input source function [*Plant*, 1982]

$$S_w(k) = m\sigma\left(\frac{u_*}{c}\right)^2 N(k), \tag{2}$$

where $m \approx 0.04$. *Phillips* [1984] shows that for gravity waves several times shorter than the spectral peak component, the nonlinear wave-wave interaction term is about an order of magnitude smaller than the other two terms. The dynamic balance of short gravity waves, therefore, is mainly determined by the input and dissipation terms. *Phillips* [1984, 1985] suggests the following formulation for the dissipation functional

$$D = gk^{-4}f(B), \tag{3}$$

where $B = k^4\Psi = k^4\sigma N/g$ is the degree of saturation. Equation (2) can be expressed in terms of B,

$$S_w(k) = m\left(\frac{u_*}{c}\right)^2 gk^{-4}B(k). \tag{4}$$

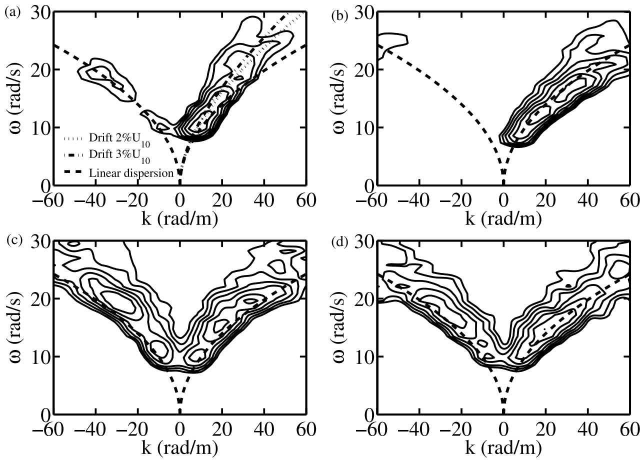

Figure 1. 2D spectra obtained by the wave gauge arrays in fixed-station (left panels) and free-drifting (right panels) configurations. The upper panels show the spectra computed from the along-wind array, and the lower panels are from the crosswind array.

At equilibrium $dN/dt = 0$. Equating equations (3) and (4) leads to the following implicit equation of $f(B)$

$$\frac{\partial B}{\partial \xi} = m\left[\frac{\partial}{\partial B}\left(\frac{f(B)}{B}\right)\right]^{-1}, \tag{5}$$

where $\xi = (u_*/c)^2$. *Phillips* [1984] concludes that if a variation of B with wind speed can be established reliably, equation (5) defines the slope of the curve $f(B)$ near equilibrium. In particular, if a power law function is assumed

$$f(B) = A_d B^{a_d}, \tag{6}$$

the exponent is

$$a_d = 1 + \frac{B}{\xi}\frac{1}{\partial B/\partial \xi}. \tag{7}$$

Experimental data (Section 4) indicate that $B(u_*/c)$ can be represented by a power law function,

$$B\left(\frac{u_*}{c}\right) = A_0\left(\frac{u_*}{c}\right)^{a_0} = A_0 \xi^{\frac{a_0}{2}}, \tag{8}$$

which leads to the following equations for a_d and A_d

$$a_d = 1 + \frac{2}{a_0}, \quad A_d = m A_0^{1-a_d}. \tag{9}$$

3. Field Experiments

[7] Field measurements are carried out to study the properties of short surface waves. The results presented here are based on u_* derived from sonic anemometers and $B(k)$ by two linear arrays of fast response capacitance wave gauges. Each array contains 20 gauges spaced 0.0508 m apart. The sensors are carried on a wave-following free-drifting buoy patterning the design by *Hwang et al.* [1996]. The free drifting operation is an important feature of this study because short waves can be easily convected by surface currents. The resulting doppler frequency shift has caused serious problems for interpreting the encounter frequency spectrum measured by fixed-station sensors. *Hwang et al.* [1996] suggest that the problem can be alleviated considerably by free drifting operation to reduce the magnitude of the current because the doppler shift is $\boldsymbol{u} \bullet \boldsymbol{k}$, where $\boldsymbol{u}$ is the current velocity. To verify the validity of the concept, the wave gauge array system is deployed in a canal approximately 100 m wide and 400 m long under fixed-station and free-drifting configurations. Figure 1 compares the 2D (k-ω) spectra, where ω is the encounter frequency (fixed-station in left panels and free-drifting in right panels). It is quite clear the doppler frequency shift problem associated with fixed-station measurements has been largely removed by free-drifting operation. The 2D spectra from crosswind array (lower panels) show the interesting feature of bimodal directional distribution of short scale waves, the main contributor to the ocean surface roughness [*Hwang and Wang*, 2001]. Further details on the measurement system and analysis procedure are reported elsewhere [*Hwang and Wang*, 2004; *Wang and Hwang*, 2004].

Table 1. Summary of the Experimental Conditions

	Population	U_{10} (m/s)	u_* (m/s)	H_s (m)	T_a (s)[a]
Subset 1	291	3.6–14.2	0.11–0.55	0.21–2.84	1.93–6.33
Subset 2	106	2.6–10.2	0.063–0.40	0.21–0.75	2.07–4.68

[a] T_a is calculated from the first moment of the wave spectrum.

[8] Wave spectra presented in this paper are collected from two field experiments conducted in 2001 and 2003. The segments of data selected for this study are limited to those with steady wind direction (±20° from the mean) and reasonably steady wind speed (±30 percent from the mean). Each raw spectrum is calculated from 163.8 s of data. The

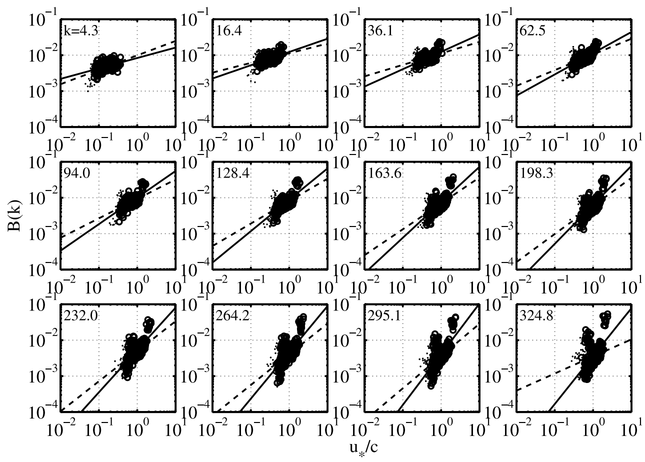

Figure 2. Scatter plots of $B(u*/c)$ for different spectral wave components, showing a power law dependence. The wavenumber is marked at the top left of each panel. Circles are for Subset 1 and dots for Subset 2. The least square fitted curves are also plotted, solid curves for Subset 1 and dashed curves for Subset 2.

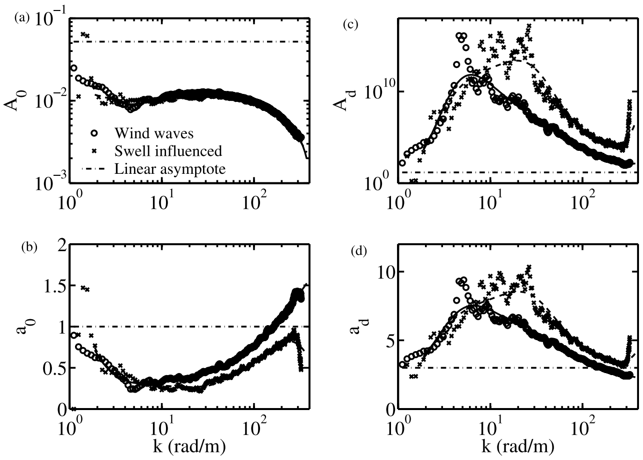

Figure 3. (a) A_0, and (b) a_0 of the empirical power law function of $B(u_*/c)$, derived from least square fitting of the data shown in Figure 2, and (c) A_d, and (d) a_d of the dissipation power law function $f(B)$ calculated from (9).

spectrum is further smoothed to yield 100 degrees of freedom. Here we focus on short waves between 0.02 and 6 m (0.5 to 12 Hz). The atmospheric stability conditions are limited to near neutral. The range of u_* is from 0.042 to 0.55 m/s. The data are further divided into two subsets (Table 1) depending on the swell influence, quantified by the ratio (R) of the spectral densities in the frequency bands $\sigma < 0.6\sigma_p$ and $\sigma \geq 0.6\sigma_p$. The first subset is dominantly wind waves with $R < 0.2$. The second subset is swell-influenced with $R \geq 0.4$.

4. Analysis Results

[9] The measured frequency spectrum is converted to the wavenumber domain using the linear dispersion relation. As shown in Figure 1, the free-drifting operation removes the doppler frequency shift problem encountered in fixed-station measurements. Also, recent analysis of spatial measurements of capillary and short gravity waves by *Zhang* [2003] and the frequency-wavenumber analysis of short waves by *Wang and Hwang* [2004] demonstrate convincingly that short waves indeed follow the linear dispersion relation. Figure 2 shows the scatter plots of $B(u_*/c)$. Representing the results by a power law function (8), A_0 and a_0 derived from least square fitting are given in Figures 3a and 3b. In the present analysis, only wave components satisfying $\omega > X\omega_p$ where $X = 2$ are included. Varying X from 1.5 to 3.0 produces only minor changes in the result. For Subset 1, the exponent a_0 is close to one in the longer wavelength region, and gradually decrease to less than 0.5, with a minimum of 0.22, for λ between 0.16 to 2.1 m. For even shorter gravity waves, the exponent slowly increases to about 1.5. The presence of swell modifies somewhat the wavenumber dependence of a_0, with its "trough" broadened, the magnitude range narrowed to between 0.22 and 1.0, and an apparent shift of the minimum value to a higher wavenumber (Figure 3b).

[10] A_d and a_d of the dissipation function (3, 6) calculated by equation (9) are shown in Figures 3c and 3d. The result shows that D approaches asymptotically to B^3 toward long gravity waves and to $B^{2.3}$ for short gravity waves. In the middle range (about $3 < k < 40$ rad/m or $0.16 < \lambda < 2.1$ m), the dependence is as strong as B^{10}, approaching a delta-function.

5. Discussions

5.1. Asymptotic Properties

[11] For both wind seas and swell-influenced conditions, the wind speed dependence of B, as reflected on the magnitude of a_0, approaches linear toward the long gravity wave region (Figure 3b). This is in general agreement with earlier investigations of the spectral coefficient and wind speed dependence of the ocean wave spectrum above the spectral peak, which can be written as

$$\chi(k) = bu_* g^{-0.5} k^{-2.5} = b\frac{u_*}{c}k^{-3}. \qquad (10)$$

The corresponding saturation spectrum is

$$B_g(k) = b\left(\frac{u_*}{c}\right). \qquad (11)$$

The range of b has been summarized by many researchers [e.g., *Toba*, 1973; *Phillips*, 1977, 1985; *Forristall*, 1981; *Donelan et al.*, 1985; *Hwang et al.*, 2000]. Based on spatial measurement of the 3D surface wave topography using an airborne scanning lidar system, $b \approx 5.2 \times 10^{-2}$ is reported by *Hwang et al.* [2000]. The present result also approaches a similar value of b in the longer wavelength region of gravity waves (Figure 3a). The resulting cubic and square dependence of $D(B)$ in gravity and capillary ends of the resolved wavenumber range are consistent with earlier theoretical analyses [*Phillips*, 1985; *Plant*, 1986].

5.2. Swell Influence

[12] The presence of swell has some influence on the observed spectral properties and the source functions (Figure 3). $B(k)$ computed by parameterized functions (Table 2) for wind waves and swell-influenced conditions are given in Figure 4a for $u_* = 0.1$, 0.2, 0.4 and 0.8 m/s. At

Table 2. Coefficients of Polynomial Fitting Equations for A_0 and a_0[a]

	P_0	P_1	P_2	P_3	P_4	P_5
			Wind Waves (Subset 1)			
A_0	-6.42×10^{-5}	-6.18×10^{-4}	-2.02×10^{-3}	-4.05×10^{-3}	-8.96×10^{-3}	1.97×10^{-3}
a_0	-2.84×10^{-3}	-3.07×10^{-2}	-1.05×10^{-1}	-1.80×10^{-2}	6.71×10^{-1}	1.52×10^{0}
			Swell Influenced (Subset 2)			
A_0	1.89×10^{-5}	3.17×10^{-4}	1.58×10^{-3}	1.66×10^{-3}	-5.05×10^{-3}	2.35×10^{-3}
a_0	-7.78×10^{-3}	-1.10×10^{-1}	-5.71×10^{-1}	-1.26×10^{0}	-8.34×10^{-1}	6.55×10^{-1}

[a] $Y = \sum_{n=0}^{N} P_n K^{N-n}$, where Y is A_0 or a_0, and $K = \log(k/k_m)$, $k_m = 374.2$ rad/m is used for normalization.

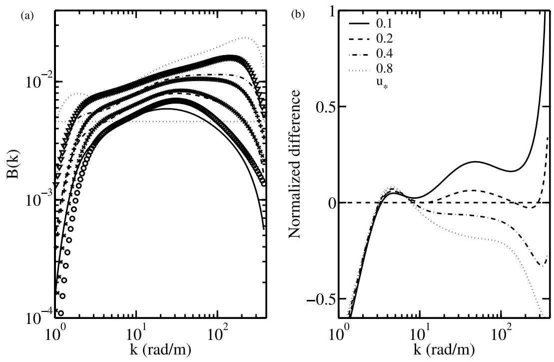

Figure 4. (a) $B(k)$ computed from the parameterization functions (Table 2): Wind-wave conditions are plotted with curves, and swell-influenced conditions are plotted with symbols. (b) The normalized difference of the saturation spectra between wind-wave and swell-influenced conditions, ΔB, which is the same as the normalized difference of the source functions, ΔS and ΔD.

equilibrium, $D(k, u_*/c) = S_w(k, u_*/c) = m(u_*/c)^2 gk^{-4} B(k, u_*)$, the source functions D and S_w can be readily constructed. Differences in the short wave spectra due to swell influence are discernable. The normalized difference is displayed in Figure 4b. For mild wind conditions ($u_* < \sim 0.2$ m/s), short waves are enhanced. At higher winds, waves shorter than $\sim$0.8 m are suppressed and middle range waves are enhanced (Figure 4b).

5.3. Implications on Wave Breaking

[13] For short gravity waves, *Banner et al.* [1989] report wavenumber spectra of surface waves measured by stereo photography. The resolved wavelengths are between 0.2 and 1.6 m ($4 \leq k \leq 31$ rad/m). The range of wind speeds is between 5.5 and 13.3 m/s. Their results indicate a very weak wind speed dependence, with $B(k) \sim u_*^{0.18}$. The results from the present analysis cover the range $0.02 \leq \lambda \leq 6$ m. For dominantly wind wave conditions, the wind speed exponent drops sharply from about 1.0 for long gravity waves to about 0.22 near $k = 5$ rad/m and remains less than 0.5 through $k = 40$ rad/m.

[14] The presence of a localized region in wavenumber space where the spectral density is only weakly dependent on the forcing wind condition is quite interesting, as it suggests a localized region where the wave growth is quenched by strong dissipation (Figures 3c and 3d). For wind-wave dominant conditions, the region of $a_0 < 0.5$ is $0.16 \leq \lambda \leq 2.1$ m. These wavelengths are sufficiently long such that viscous dissipation or parasitic capillary generation as an energy sink mechanism may be neglected. Wave breaking as the major dissipation mechanism can be reasonably assumed. Does the observation of a localized wavenumber region of distinctive change of the dissipation function suggest that the length scale of breaking wind waves is localized in the range of about 0.16 to 2.1 m, and that the presence of swell broadens the breaking scales? If so, this represents a useful piece of information for refining our whitecapping source function used in numerical models of wind wave generation and evolution. The result support many years of microwave observations of the ocean surface, all of which seem to indicate that doppler shifts at HH polarization and low incidence angles are due to scatterers traveling at the speed of surface waves with lengths of a few meters [e.g., *Plant*, 1997; Plant, personal communication, 2004]. Presently, we do not have reliable information on the spectral composition of breaking waves and the techniques to make such observations. The approach designed by *Phillips* [1984] and radar remote sensing may prove to be quite useful for deriving key information of breaking waves.

6. Summary

[15] The determination of the dissipation function in the wave action conservation equation remains one of the most difficult tasks in surface wave studies. *Phillips* [1984] suggests an approach to quantify the dissipation function in the equilibrium range through the functional dependence of $B(u_*/c)$, as briefly described in Section 2. A series of field experiments is analyzed to quantify $B(u_*/c)$. The results show that for short waves in the equilibrium range the wave spectral function follows closely the power law relationship, with its exponent approaching asymptotically to 1.0 and 1.5, respectively, toward the lower and higher wavenumber ranges of the dataset. In the middle range ($0.16 \leq \lambda \leq 2.1$ m), the wind speed dependence is much weaker. The dissipation function in the equilibrium region (equation (3)) can then be calculated by equations (6) and (9). The dependence of D on B is about cubic for $\lambda > \sim 6$ m and close to square for $\lambda \leq \sim 0.02$ m. In the middle range, a much stronger power law dependence (as high as B^{10}) is found (Figure 3d). The result indicates a localized (in wavenumber domain) region where the dissipation function displays a drastic change and approaches a delta-function. A feasible explanation of the change is attributed to wave breaking. It is inferred from this result that the spectral property of wave breaking is localized in the wavenumber space, with special features (yet to be determined) in the 0.16 to 2.1 m wavelength scale. In the presence of swell, the localization is more smeared, and the length scale of features moves toward shorter wave components.

[16] **Acknowledgments.** This work is sponsored by the Office of Naval Research (NRL PE 61153N). Ray Burge and Richard Smith assist in the preparation and execution of the field experiments. The captain and crew onboard R/V Longhorn provide the critical logistics support. Naval Research Laboratory contribution JA/7330—04-0005.

References

Banner, M. L., I. S. F. Jones, and J. C. Trinder (1989), Wavenumber spectra of short gravity waves, *J. Fluid Mech.*, *198*, 321–344.

Donelan, M. A., J. Hamilton, and W. H. Hui (1985), Directional spectra of wind-generated waves, *Philos. Trans. R. Soc. London, Ser. A*, *315*, 509–562.

Forristall, G. Z. (1981), Measurements of a saturated range in ocean wave spectra, *J. Geophys. Res.*, *86*, 8075–8084.

Hwang, P. A., and D. W. Wang (2001), Directional distributions and mean square slopes in the equilibrium and saturation ranges of the wave spectrum, *J. Phys. Oceanogr.*, *31*, 1346–1360.

Hwang, P. A., and D. W. Wang (2004), Field measurements of duration limited growth of wind-generated ocean surface waves at young stage of development, *J. Phys. Oceanogr.*, in press.

Hwang, P. A., S. Atakturk, M. Sletten, and D. B. Trizna (1996), A study of the wavenumber spectra of short water waves in the ocean, *J. Phys. Oceanogr.*, *26*, 1266–1285.

Hwang, P. A., D. W. Wang, E. J. Walsh, W. B. Krabill, and R. N. Swift (2000), Airborne measurements of the directional wavenumber spectra of ocean surface waves. Part 1. Spectral slope and dimensionless spectral coefficient, *J. Phys. Oceanogr.*, *30*, 2753–2767.

Phillips, O. M. (1977), *The Dynamics of the Upper Ocean*, 2nd ed., 336 pp., Cambridge Univ. Press, New York.

Phillips, O. M. (1984), On the response of short ocean wave components at a fixed wavenumber to ocean current variations, *J. Phys. Oceanogr.*, *14*, 1425–1433.
Phillips, O. M. (1985), Spectral and statistical properties of the equilibrium range in wind-generated gravity waves, *J. Fluid Mech.*, *156*, 505–531.
Plant, W. J. (1982), A relationship between wind stress and wave slope, *J. Geophys. Res.*, *87*, 1961–1967.
Plant, W. J. (1986), A two-scale model of short wind-generated waves and scatterometry, *J. Geophys. Res.*, *91*, 10,735–10,749.
Plant, W. J. (1997), A model for microwave Doppler sea return at high incident angles: Bragg scattering from bound, tilted waves, *J. Geophys. Res.*, *102*, 21,131–21,146.
Toba, Y. (1973), Local balance in the air-sea boundary processes. III. On the spectrum of wind waves, *J. Phys. Oceanogr.*, *3*, 579–593.
Wang, D. W., and P. A. Hwang (2004), On the dispersion relation of short gravity waves from space-time wave measurements, *J. Atmos. Oceanic Technol.*, in press.
Zhang, X. (2003), Surface image velocimetry for measuring short wind wave kinematics, *Exp. Fluids*, *35*, 653–665.

P. A. Hwang and D. W. Wang, Oceanography Division, Naval Research Laboratory, Stennis Space Center, MS 39529, USA. (phwang@nrlssc.navy.mil)